

# Near-field probing of photonic crystals

**E. Flück<sup>1</sup>, M. Hammer<sup>2</sup>, W.L. Vos<sup>3</sup>, N.F. van Hulst<sup>1</sup>, and L. Kuipers<sup>1,4</sup>**

<sup>1</sup>*Applied Optics, MESA<sup>+</sup> Institute for Nanotechnology and Dept. of Science & Technology, University of Twente, P.O. Box 217, 7500 AE Enschede, The Netherlands*

<sup>2</sup>*Applied Analysis and Mathematical Physics, MESA<sup>+</sup> Institute for Nanotechnology and Dept. of Electrical Engineering, Mathematics and Computer Sciences, University of Twente, P.O. Box 217, 7500 AE Enschede, The Netherlands*

<sup>3</sup>*Complex Photonic Systems, MESA<sup>+</sup> Institute for Nanotechnology and Dept. of Science & Technology, University of Twente, P.O. Box 217, 7500 AE Enschede, The Netherlands*

<sup>4</sup>*FOM Institute for Atomic and Molecular Physics (AMOLF), Kruislaan 407, 1098 SJ Amsterdam, The Netherlands*

## ABSTRACT

Photonic crystals form an exciting new class of optical materials that can greatly affect optical propagation and light emission. As the relevant length scale is smaller than the wavelength of light, sub-wavelength detection forms an important ingredient to obtain full insight in the physical properties of photonic crystal structures. Spatially resolved near-field measurements allow the observation of phenomena that remain hidden to diffraction-limited far-field investigations. Here, we present near-field investigations in both collection- and illumination mode that highlight the power of local studies. We show how propagation losses are unambiguously determined and that light detected in far-field transmission can actually contain contributions from different, sometimes unexpected, local scattering phenomena. Simulations are used to support our findings. Furthermore, it is shown that local coupling of light to a thick three-dimensional photonic crystal is position-dependent and that the spatial distribution of the coupling efficiency itself is frequency-dependent.

**PACS:** 42.70.Qs, 42.25.Bs, 07.79.Fc

**Keywords:** Near-field optics, photonic crystals, microscopy, scattering, losses, coupling

## Corresponding author:

L. Kuipers

Kruislaan 407

1098 SJ Amsterdam

The Netherlands

Tel: +31-20-6081234

Fax: +31-20-6684106

e-mail: L.Kuipers@amolf.nl

## 1. INTRODUCTION

Photonic crystals form a powerful new class of optical materials that offer a large potential for applications and fundamental science as they can affect both optical propagation and the spontaneous emission of light by embedded sources [1,2]. Photonic crystals are rarely considered as the complex photonic structure they are; their full description should take into account not only their far-field properties but also their near-field properties [3]. By far the most utilized approach for investigating photonic crystal structures are transmission and reflection experiments, see e.g. Refs. 4-5. There, both the source and the detector are in the far-field and hence near-field properties remain hidden. The second approach studies spontaneous emission of sources inside the crystals that probe the so-called local density of states (LDOS) [1,2]. The LDOS contains both far-field and near-field properties. In both approaches the optical properties are spatially averaged or contain contributions of many different emitters by virtue of the fact that the detector is in the far-field.

In other words all conventional techniques are limited by the fact that they cannot yield information below the diffraction limit. For example, the propagation of light inside photonic crystal structures is impossible to investigate with far-field techniques for two reasons. Firstly, by their very nature the highest attainable resolution is limited to roughly  $\lambda/2$ . Secondly, light inside photonic crystal structures can have wavevectors that are larger than light outside the structure, but with the same optical frequency, would have. As a result, this light is evanescent outside the structure, exponentially decaying with the distance from the structure. As a result light with such wavevectors can, by definition, not be observed by far-field techniques.

Local and near-field properties of photonic crystals can be investigated with near-field optical microscopy [6-8]. So far, only a few such studies exist, see e.g. Refs. 9-12. Here, we present two examples of near-field optical investigations of photonic crystals that focus on phenomena that would have remained hidden in far-field studies. In the first we study losses and unexpected scattering phenomena around a finite-sized one-dimensional photonic crystal structure. In the second we investigate near-field coupling from point-like light source to a thick three-dimensional photonic crystal.

## **2. NEAR-FIELD MICROSCOPY**

Two main configurations exist for near-field microscopy: the collection mode and the illumination mode [6]. Of each of these two main configurations several variations exist. In the following we will focus on the set-ups used for the investigations presented here.

### **2.1 Collection mode**

As near-field optical microscope in collection mode we use a so-called Photon Scanning Tunnelling Microscope (PSTM) [13]. Figure 1 shows the schematic of a PSTM. Light is guided in a structure and an evanescent field is present above the structure's surface. The evanescent field is frustrated by a sub-wavelength probe that is brought into close proximity with the sample surface. As a result, the evanescent field can couple to guided modes of the probe. Thus, a small fraction of the evanescent field is picked up and subsequently detected with a sensitive (photon) detector. By raster scanning the probe over the photonic structure a map can be constructed of the intensity distribution in the structure. The resolution of this map is determined by the size of the probe, which is sub-wavelength in all our investigations. To keep the probe-surface separation constant a shear force height feedback is used. As the probe-sample separation is kept constant, while the probe is scanned across the structure, the height feedback yields a map of the topography. Figure 1 also shows the interferometric branches that allow phase-sensitive near-field measurement. The phase sensitivity was not used in this investigation.

### **2.2 Illumination mode**

In illumination mode the sub-wavelength aperture of a near-field probe is used as a small light source. Figure 2 schematically depicts the instrument used to investigate local optical coupling to three-dimensional photonic crystals. The 200  $\mu\text{m}$ -thick photonic crystal sample is illuminated by the sub-wavelength aperture [14] of a near-field optical probe. The light that is coupled to the crystal and which subsequently propagates through the crystal to the other side is collected by a large photodetector at the rear of the sample. The size of the detector is much larger than the size of the crystal. As a result, all light emerging from the back of the crystal is collected by the detector. It is

useful to point out that the mean free path of light diffusion ( $15\ \mu\text{m}$ ) of the crystal is shorter than the thickness of the crystal. The light that propagates through and exits from the crystal is therefore randomised and independent of the position of the probe. Consequently, all light with the large range of wavevectors that is launched from the sub-wavelength tip into the crystal is ultimately detected. The probe-sample separation ( $z$ ) of the probe is controlled in either of two ways. First,  $z$  is controlled with a shear-force height feedback similar to the one used in the PSTM (constant gap mode). This way a topographical contour of the crystal surface is scanned. Secondly, the aperture is scanned in a single plane parallel to the crystal surface at a constant, fixed height (constant height mode).

### **3. NEAR-FIELD STUDY OF A ONE-DIMENSIONAL PHOTONIC CRYSTAL STRUCTURE**

#### **3.1 Near-field measurements**

The basis for the one-dimensional photonic crystal structure (1DPhCS) is a  $\text{Si}_3\text{N}_4$  ridge waveguide, grown on top of a  $\text{SiO}_2$  layer ( $3.2\ \mu\text{m}$  thick) on top of a Si substrate. The ridge height is 11 nm and the  $\text{Si}_3\text{N}_4$  slab layer has a thickness of 44 nm. The width of the waveguide is  $1.5\ \mu\text{m}$ . The photonic crystal structure is fabricated through direct sputtering with focused ion beam. [15] Its period is 220 nm and the slits are 110 nm wide and  $2.5\ \mu\text{m}$  long. The depth of the slits is at least 70 nm, i.e. the  $\text{Si}_3\text{N}_4$  slab layer is fully penetrated.

Figure 3 shows a PSTM measurement of light ( $\lambda_0 = 610\ \text{nm}$ ) in and around a one-dimensional photonic crystal structure. The top panel shows the measured topography. The 11 nm high ridge is clearly visible as is the period slit structure forming the one-dimensional photonic crystal structure. The horizontal stripes in the topographical image are caused by environmental changes [16]. The bottom panel depicts the measured intensity distribution. Light is incident from the bottom of the picture. In front of the array a clear horizontal pattern is visible with a period of 223 nm. This sub-wavelength intensity pattern is obviously caused by interference of the incident light with light reflected from the one-dimensional photonic crystal structure. It is clear that the small period of this pattern precludes its observation with far-field techniques. Inside the one-dimensional photonic crystal structure the periodic pattern is still visible, but the optical intensity decreases further into the structure. Unexpectedly, a recovery of the optical intensity is evident behind the grating. Moreover,

the recovered intensity in the waveguide exhibits minima and maxima. It is interesting to note that the minima and the maxima are not equidistant.

Figure 4 shows a line trace of the measured optical intensity along the waveguide. To enhance the signal-to-noise ratio all scan lines are summed over a 1  $\mu\text{m}$  wide area in the middle of the waveguide. In the left part of the graph oscillations due to the standing wave in front of the one-dimensional photonic crystal structure are visible. Inside the one-dimensional photonic crystal structure the intensity rapidly decays. Behind the structure the non-periodic recovery is evident. At the location of the first slit a high intense peak spike is observed. The peak can be 2.5x as high as that of the incoming light. We attribute this high intensity to light that is scattered directly from the one-dimensional photonic crystal structure into the probe due to the abrupt transition from the ridge waveguide to the one-dimensional photonic crystal structure.

In the region of the photonic crystal structure a periodic pattern is also visible with a period (220 nm) that corresponds directly to that of the one-dimensional photonic crystal structure. This period is observed for all colors used in this study. The difference between this period and that of the standing wave in front of the structure can only be observed via a Fourier analysis. The fact that the periodicity of the light inside the crystal conforms to the crystal period is consistent with the observation of Bloch modes. By fitting an exponentially decaying function ( $I(x) \propto \exp(-\beta x)$ ) to the intensity maxima inside the structure, the losses of the structure can be determined without any additional data interpretation.

### **3.2 Simulation results**

The optical fields inside the photonic crystal structure have been calculated with a 2D simulation based on solving Maxwell's equations in the frequency domain [17-18]. Figure 5 depicts the calculated distribution of  $|E_{\perp}|^2$  for a cross section through the waveguide region containing the 15 slits with a logarithmic grayscale for the intensities, where bright and dark represent high and low intensities, respectively. The  $E_{\perp}$  component is equivalent to the TE polarization that was launched into the structure. The calculation take into account the layer package used in the experiment, i.e. a 55 nm layer of  $\text{Si}_3\text{N}_4$  on top of a 3.2  $\mu\text{m}$  thick  $\text{SiO}_2$  layer. For the wavelengths used in this investigation the reflection at the  $\text{SiO}_2$ -Si interface is appreciable. This interface is therefore mimicked by a perfect

mirror. In front of the slits a strong periodic pattern is observed, corresponding to the standing waves caused by the interference between incoming light and light reflected from the slits. Inside the slit region the period of  $|E_{\perp}|^2$  is the same as the crystal period.

The calculations also show the origin of the non-periodic recovery observed behind the one-dimensional photonic crystal structure. Not only is light at the first slit scattered back into the waveguide; it is also scattered into the SiO<sub>2</sub> substrate. The light scattered into the substrate is subsequently reflected at the Si-SiO<sub>2</sub> interface at a depth of -3.2 μm. As a result, an interference pattern is formed between light still in the waveguide after the photonic structure and light scattered from the Si-substrate interface. In order to compare the calculations with the near-field measurements the calculated  $|E_{\perp}|^2$  distribution at a height of 10 nm above the waveguide is used as this is the typical height of the PSTM probe in the measurement.

### 3.3 Discussion

Figure 6 compares the intensity decay rates, i.e. the losses, inside the structure for different incident wavelengths as determined with the near-field optical measurements with those obtained from the simulations. The decay rates  $\beta$  correspond to losses ranging from 4.4 dB/μm to 11.4 dB/μm. It is clear that a good agreement is found between experiment and simulations. We find that the losses increase with decreasing wavelength. This wavelength dependence is consistent with the wavelength dependence of losses caused by scattering.

Both simulations and measurements exhibited a non-periodic recovery in the waveguide behind the structure. The simulations indicated that light can scatter from the first slit into the substrate and subsequently reflect from the buried Si-SiO<sub>2</sub> interface. Combined with the remaining light transmitted by the one-dimensional photonic crystal structure this light set up a non-periodic interference pattern. Recent simulations show that a large fraction of the light remaining in the waveguide after the one-dimensional photonic crystal structure, bypasses the crystal structure via the substrate but without reflecting from the substrate. Both in measurements and in simulations we have determined the positions  $\Delta x_i$  with respect to the last slit of the minima of the pattern for several wavelengths. Figure 7 compares the measured and the calculated positions of the minima. An excellent agreement is found

between experiment and calculation. Our observations show that light in photonic devices can sometimes bypass structures aimed at manipulating the light. In principle, this type of behaviour can lead unwanted cross talk in complex photonic crystal devices.

#### 4. LOCAL COUPLING TO THREE-DIMENSIONAL PHOTONIC CRYSTALS

Where near-field optics in collection mode detects light already present in a photonic structure, near-field optics can also be used to launch light into a structure and obtain sub-wavelength information on the coupling process. [19] Figure 8 shows the transfer of light ( $\lambda_0 = 647$  nm) that is launched from a sub-wavelength sized aperture into a thick three-dimensional photonic crystal and detected at the back of the crystal. Figure 8a shows the topography determined simultaneously with figure 8b when the height feedback is engaged. The periodically ordered arrangement of polystyrene spheres (diameter = 482 nm) that make up the  $\langle 111 \rangle$ -facet of the photonic crystal is clearly visible. A minor topographical tip convolution is also apparent.

Figures 8b-e show the detected optical signal when the tip is scanned across the  $\langle 111 \rangle$ -facet at different heights ( $z$ ). The heights range from  $z = 10 \pm 5$  nm (Fig. 8b) when the tip is in shear-force feedback, to  $z = 84 \pm 30$  nm (Fig. 8c), to  $z = 446 \pm 30$  nm, and finally  $z = 723 \pm 16$  nm (constant height mode [20]). For investigated values of  $z$  a clear hexagonal pattern of bright spots is visible. It is also evident that the topographical tip convolution effects are not reproduced in the optical signal. We can therefore exclude topographical artefacts, such as those categorised, e.g., by Hecht *et al.* [21]. The period of the optical pattern is identical to that of the crystal structure and more light is coupled to the crystal when the aperture is above a sphere. The contrast in the image clearly varies on sub-wavelength length scales of  $\sim 100$  nm, that is,  $\lambda/7$ . Note, that our method therefore reveals near-field information concerning the coupling mechanism.

The optical modulation, defined as  $M = (I_{\max} - I_{\min}) / (I_{\max} + I_{\min})$ , of the detected signal at the smallest height is 7% and decreases to 4% at the largest height. The average detected intensity drops by 13% as the height is increased from  $\sim 10$  nm to 723 nm. Thus, more light is coupled into the photonic crystal

when the probe is in the near-field regime. The increase in throughput in the near-field regime strongly indicates that wavevectors beyond the critical angle are coupled into the photonic crystal.

The experiment is repeated for two more incident wavelengths, so in total the experiment is carried out for  $\lambda_0 = 647$  nm, 568 nm and 514 nm. The  $\lambda_0 = 647$  nm is situated below the second order L-gap of the crystal near 600 nm, whereas the two shorter wavelengths are located inside the stopgap region. Figure 9 shows the optical patterns measured for the 3 incident wavelengths. For all wavelengths a clear hexagonal pattern with a period of the  $\langle 111 \rangle$ -facet is observed. However, clear differences are observed when the optical pattern obtained for  $\lambda_0 = 647$  nm is compared to the patterns obtained for  $\lambda_0 = 568$  nm and 514 nm. Firstly, the bright spots decrease slightly in size. The width of the spots is 370 nm for  $\lambda_0 = 647$  nm and 280 nm for  $\lambda_0 = 568$  nm and 514 nm. In addition, the shape of the spots also changes. But more importantly, the “center-of-mass” (CoM) of the bright spots shifts with respect to the underlying topographical lattice. A quantitative analysis shows that the CoM shifts by  $82 \pm 6$  nm along the  $\langle \bar{1}10 \rangle$ -direction and by  $24 \pm 9$  nm along the  $\langle \bar{1}01 \rangle$ -direction when the wavelength is changed from 647 nm to 514 nm. When the wavelength is changed from 647 nm to 568 nm the shifts along these directions are  $72 \pm 6$  nm and  $23 \pm 9$  nm, respectively.

We propose a tentative explanation for the observed changes in optical patterns as the wavelength is varied. The origin of the complex and asymmetric patterns is ascribed to the influence of the second-order stopgap region near 600 nm. The optical frequency corresponding to  $\lambda_0 = 647$  nm lies well below the stopgap. For this wavelength propagating Bloch modes can be excited. These Bloch modes require the same symmetry as the crystal, which is clearly observed in our measurements. For the other two wavelengths ( $\lambda_0 = 568$  nm and 514 nm), the corresponding frequencies lie in the stopgap so no Bloch modes exist in the  $\Gamma L$  direction in reciprocal space. For frequencies in the stopgap, the intensity distribution doesn't have the symmetry of the underlying crystals, and it shifts through the unit cell. This hypothesis follows reasoning from diffraction theory for X rays [22].

A full understanding of the observed coupling behaviour as a function of wavelength will encompass all crystallographic directions to which a sub-wavelength source can couple in addition to the  $\Gamma L$ -direction. It is likely to incorporate a scattering formalism used to describe scanning tunnelling

microscopy [23] and therefore will also contain the role of the local density of states in coupling like from a point source to a photonic structure [24]. It is anticipated that new finite difference time domain [25] will help to shed light on the new insight about local light transfer as described in this work.

## 5. CONCLUSIONS

Near-field optical studies reveal local optical phenomena that remain hidden in far-field studies. Near-field microscopy in collection mode allows a direct determination of losses inside photonic crystal structures. This determination is unambiguous and model-independent. We observe that light can bypass a one-dimensional photonic crystal structure. This phenomenon could lead to unwanted cross-talk in complex photonic crystal devices. We have shown that the near-field coupling from a point-like source to a three-dimensional photonic crystal depends on the relative position of the source to the crystal surface on sub-wavelength length scales. For optical frequencies in the vicinity of an L-gap, the spatial patterns change position and shape as a function of frequency.

## ACKNOWLEDGEMENTS

The authors thank Lydia Bechger and Bert Otter for the fabrication of the samples and Jeroen Korterik for technical support on the near-field microscope. This research is part of the Strategic Research Orientation on Advanced Photonic Structures of the MESA<sup>+</sup> Institute for Nanotechnology. Furthermore, this work is part of the research program of the Stichting voor Fundamenteel Onderzoek der Materie (FOM), which is financially supported by the Nederlandse Organisatie voor Wetenschappelijk Onderzoek (NWO).

## REFERENCES

1. *Photonic Crystals and Light Localization in the 21<sup>st</sup> Century, Vol. 563 of NATO Advanced Studies Institute, Series C: Mathematical and Physical Sciences*, edited by C.M. Soukoulis (Kluwer, Dordrecht, 2001).

2. K. Sakoda, *Optical Properties of Photonic Crystals*, Springer Series in Optical Sciences, Vol. 80 (Springer, New York, 2001).
3. J.D. Jackson, *Classical Electrodynamics* (Wiley, New York, 1998).
4. P. Mach, P. Wiltzius, M. Megens, D.A. Weitz, K.H. Lin, T.C. Lubensky, and A.G. Yodh, *Phys. Rev. E* **65**, 031720 (2002), and references therein.
5. A.F. Koenderink, L. Bechger, H.P. Schriemer, A. Lagendijk, and W.L. Vos, *Phys. Rev. Lett.* **88**, 143903 (2002).
6. M.A. Paesler, and P.J. Moyer, *Near-field optics: theory, instrumentation, and applications* (Wiley, New York, 1996).
7. *Nano-Optics*, edited by S. Kawata, M. Ohtsu, M. Irie, and M. Ohtsu (Springer, Berlin 2002).
8. D. Courjon, *Near-field Microscopy and Near-field Optics* (Imperial college press, London, 2003)
9. P.L. Phillips, *et al.*, *J. Appl. Phys.* **85**, 6337 (1999).
10. S.I. Bozhevolnyi, *et al.*, *Phys. Rev. B* **66**, 235204 (2002).
11. K. Okamoto, *et al.*, *Appl. Phys. Lett.* **82**, 1676 (2003).
12. P. Kramper, *et al.*, *Phys. Rev. Lett.* **92**, 113903 (2004).
13. M.L.M. Balistreri, J.P. Korterik, G.J. Veldhuis, L. Kuipers, and N.F. van Hulst, *J. Appl. Phys.* **89**, 3307 (2001).
14. J.A. Veerman, A.M. Otter, L. Kuipers, and N.F. van Hulst, *Appl. Phys. Lett.* **72**, 3115 (1998).
15. C. Peeters, E. Flück, M.L.M. Balistreri, A.M. Otter, L. Kuipers, and N.F. van Hulst, *Appl. Phys. Lett.* **77**, 142 (2000).
16. E. Flück, M. Hammer, A.M. Otter, J.P. Korterik, L. Kuipers, and N.F. van Hulst, *J. Lightwave Technol.* **21**, 1384-1393 (2003).
17. M. Lohmeyer and R. Stoffer, *Opt. Quantum Electron.* **33**, 413 (2001).
18. M. Lohmeyer, *Opt. Quantum Electron.* **34**, 541 (2002).
19. E. Flück, N.F. van Hulst, W.L. Vos, and L. Kuipers, *Phys. Rev. E (Rapid Communication)* **68**, 015601 (2003).

20. M.L.M. Balistreri, J.P. Korterik, L. Kuipers, and N.F. van Hulst, *Appl. Phys. Lett.* **77**, 4092 (2000).
21. B. Hecht, H. Bielefeldt, Y. Inoue, and D.W. Pohl, *J. Appl. Phys.* **81**, 2492 (1997).
22. R.W. James, *The Optical Principles of the Diffraction of X-rays* (Bell, London, 1954).
23. R. Carminato and J.J. Saenz, *Phys. Rev. Lett.* **84**, 5156 (2000).
24. G. Colas de Francs et al., *Phys. Rev. Lett.* **86**, 4950 (2001).
25. J.S. Kole, M.T. Figge, and H. De Raedt, *Phys. Rev. E* **64**, 066705 (2001).

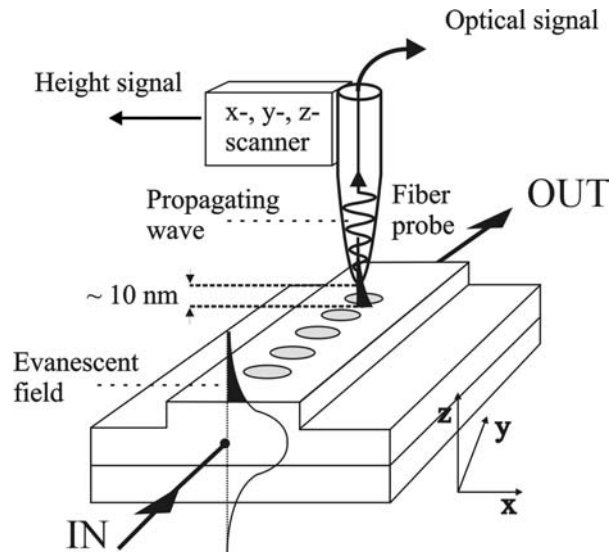


Figure 1. Schematic depiction of a Photon Scanning Tunnelling Microscope (PSTM), i.e. a near-field microscope in collection mode. Light propagates in a light guiding structure and above the surface of the structure an evanescent field is present. A nanoscopic fiber probe is kept at a constant height ( $\sim 10$  nm) above the sample surface and frustrates the evanescent field. As a result part of the evanescent field is coupled to the propagating modes of the fiber probe. This light is picked up and subsequently detected. The height feedback loop used to keep the probe-sample separation constant yields the topographic map of the structure under investigation.

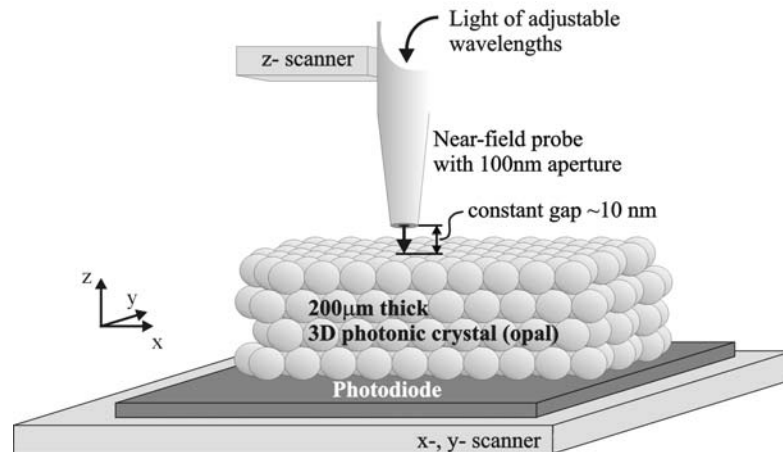


Figure 2. Schematic depiction of the illumination mode near-field optical microscope used for measuring the local coupling of fields to a thick ( $200\ \mu\text{m}$ ) three-dimensional photonic crystal. Light from the sub-wavelength aperture of a near-field probe is incident on the three-dimensional photonic crystal. By scanning the probe relative to the surface of the photonic crystal, the local light transfer is measured. All the light reaching the end of the crystal is collected by a large photodiode mounted below the crystal.

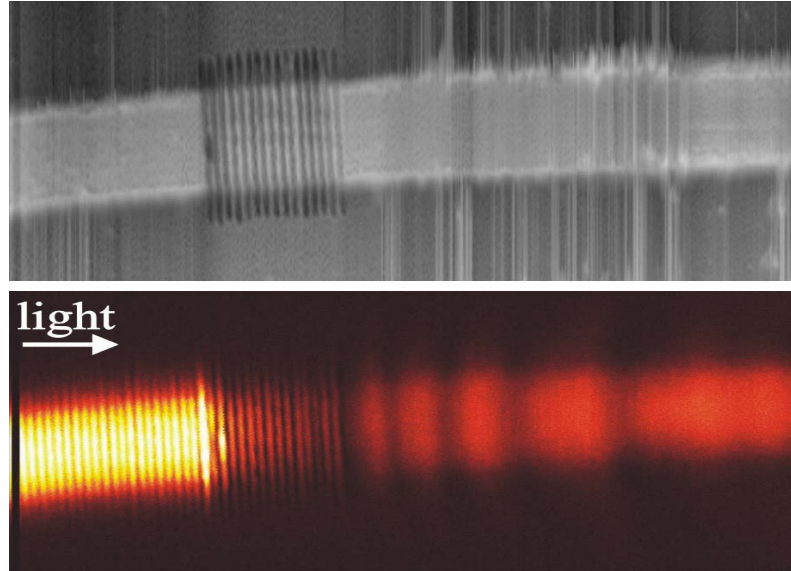


Figure 3. PSTM measurement on a periodic structure of 15 slits in a ridge waveguide (Image size  $4.0 \times 18.3 \mu\text{m}^2$ ). (top) The topographical image recorded simultaneously with the optical image. The periodic arrangement of slits is clearly resolved. The periodicity of the structure is 220 nm. The width and length of the slits are 110 nm and 2500 nm, respectively. (bottom) The optical field distribution. The light ( $\lambda_0 = 610 \text{ nm}$ ) is incident on the structure from the left. Just in front of the structure a horizontal pattern with a period of  $\sim 210 \text{ nm}$  is visible. Inside the slit region the field rapidly decays. Behind the structure a spatially modulated recovery of optical field is evident.

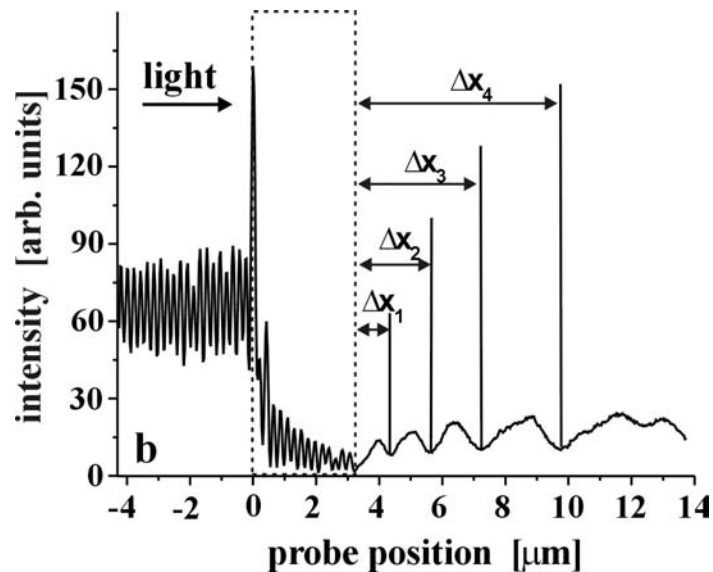


Figure 4. Line trace of the optical intensity in figure 3. To increase the signal-to-noise several adjacent line traces through the center of the waveguide were averaged. The arrow indicates the incident direction of the light. The dotted square indicates the position of the slit array. The standing waves visible in figure 3 are visible in front of the array. The modulated optical recovery is clear behind the array. The distances  $\Delta x_i$  denote the distance between the minima in the recovery pattern and the final slit of the array.

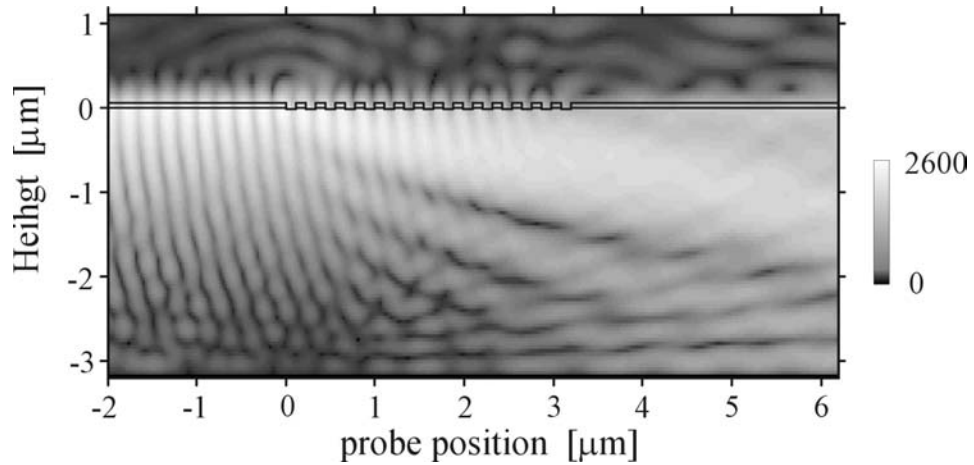


Figure 5. Grayscale (logarithmic intensity scale) representation of the simulated spatial distribution of  $|E_{\perp}|^2$  of a waveguide containing 15 slits. The simulation is two-dimensional. The structure is depicted with the drawn lines.  $E_{\perp}$  is the field component perpendicular to the simulation plane. The light is incident from the left. In front of the array a standing wave pattern is evident. Behind the structure (right side of the image) an interference pattern is visible just above the ridge waveguide. The simulation shows that this pattern is caused by an interference of light propagating through the array and light that is scattered by the front slit towards the substrate and subsequently reflected from that same substrate.

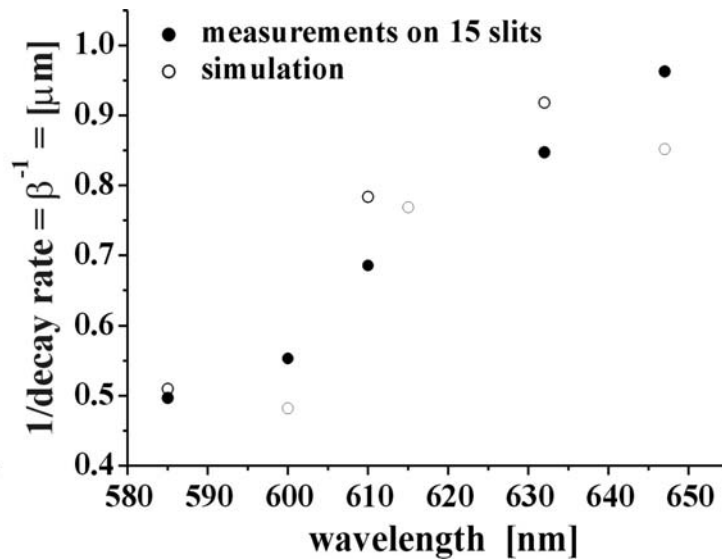


Figure 6. Measured and calculated decay rates of the optical intensity inside the periodic array of slits as a function of wavelength. A good agreement is found between the measurements and the calculations. In both cases a fit with  $\exp(-\beta x)$  was performed on the intensity line traces.

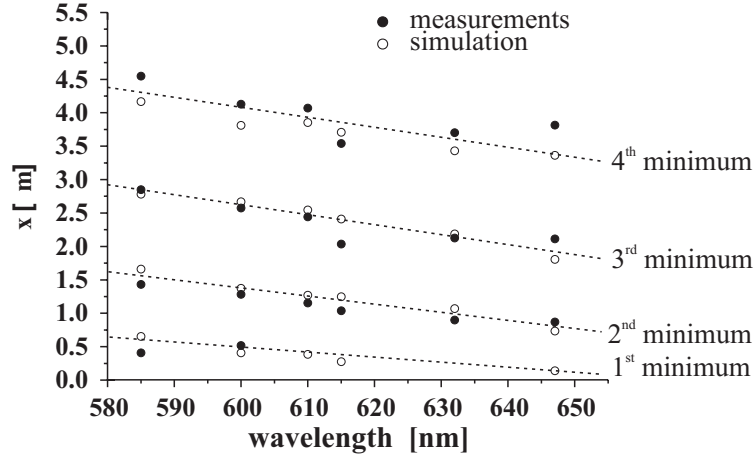


Figure 7. Measured (see figure 4) and calculated distance between the final slit and the minima in the recovery pattern behind the array as a function of wavelength. The recovery pattern is non-periodic as the distance between successive minima increases. Good agreement between measurement and calculation is found.

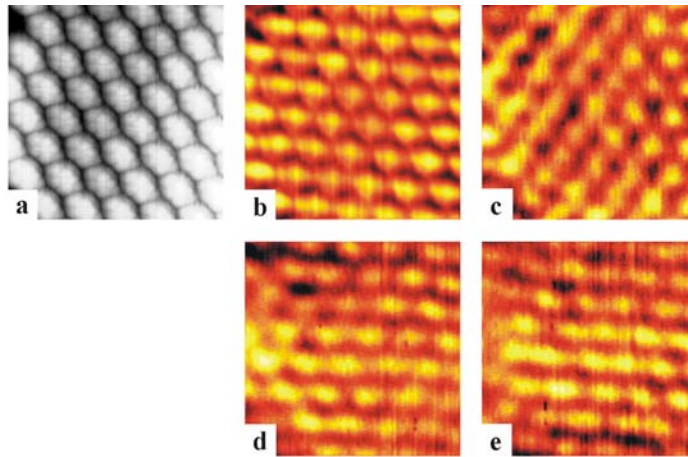


Figure 8. Near-field measurements of optical coupling from a sub-wavelength aperture to a three-dimensional photonic crystal for different aperture-surface separations (Image size:  $2.71 \times 3.02 \mu\text{m}^2$ ). a. Topographical image, the hexagonal arrangement of the  $\langle 111 \rangle$  facet of the crystal is visible. b-e. Detected intensity at the back of the crystal as a function of the x-y position. b. Distance above the surface  $z \sim 10$  nm in shear-force feedback; optical information is simultaneously measured with a. c-e. Detected spatial intensity distributions for planes parallel to the  $\langle 111 \rangle$ -facet at  $z = 84$  nm,  $z = 446$  nm and  $z = 723$  nm, respectively. The optical patterns show a clear spatial dependence for the coupling to the three-dimensional crystal. The spatial pattern persists as the surface-aperture is increased.

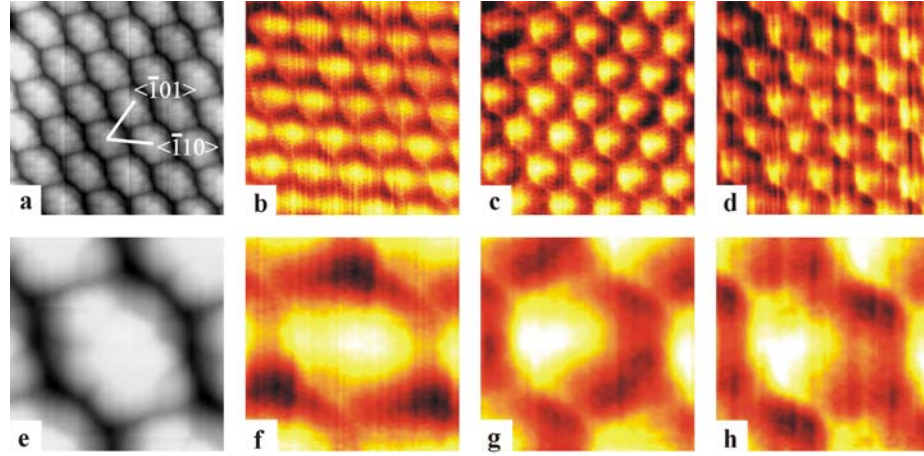


Figure 9. Position-dependent optical coupling of light from a sub-wavelength aperture to a three-dimensional photonic crystal obtained for different incident optical wavelengths. a. Topographical information of the  $\langle 111 \rangle$ -facet. b.-d. Measured near-field optical transfer patterns at  $\lambda_0 = 647$  nm, 568 nm and 514 nm, respectively. Image sizes:  $2.71 \times 3.02 \mu\text{m}^2$  e.-h. Close-up of the images a.-d. depicting roughly one unit cell. The images depict an averaged unit cell to highlight the details in the original measurements. Image size  $0.65 \times 0.72 \mu\text{m}^2$ .